10674 *Biochemistry* **2010,** *49,* 10674–10681
DOI: 10.1021/bi101590c

BIOCHEMISTRY
including biophysical chemistry & molecular biology
Article

The Cys319 Loop Modulates the Transition between Dehydrogenase and Hydrolase Conformations in Inosine 5′-Monophosphate Dehydrogenase†

Helen R. Josephine,‡ Kanchana R. Ravichandran,§,⊥ and Lizbeth Hedstrom*,‡,∥

‡*Department of Biology,* §*Department of Biochemistry, and* ∥*Department of Chemistry, Brandeis University, Waltham, Massachusetts 02454-9110, United States.* ⊥*Current address: Department of Chemistry, Massachusetts Institute of Technology, 77 Massachusetts Ave., Cambridge, MA 02139.*

Received September 30, 2010; Revised Manuscript Received November 8, 2010

ABSTRACT: X-ray crystal structures of enzyme−ligand complexes are widely believed to mimic states in the catalytic cycle, but this presumption has seldom been carefully scrutinized. In the case of *Tritrichomonas foetus* inosine 5′-monophosphate dehydrogenase (IMPDH), 10 structures of various enzyme−substrate−inhibitor complexes have been determined. The Cys319 loop is found in at least three different conformations, suggesting that its conformation changes as the catalytic cycle progresses from the dehydrogenase step to the hydrolase reaction. Alternatively, only one conformation of the Cys319 loop may be catalytically relevant while the others are off-pathway. Here we differentiate between these two hypotheses by analyzing the effects of Ala substitutions at three residues of the Cys319 loop, Arg322, Glu323, and Gln324. These mutations have minimal effects on the value of k_{cat} (≤5-fold) that obscure large effects (> 10-fold) on the microscopic rate constants for individual steps. These substitutions increase the equilibrium constant for the dehydrogenase step but decrease the equilibrium between open and closed conformations of a mobile flap. More dramatic effects are observed when Arg322 is substituted with Glu, which decreases the rates of hydride transfer and hydrolysis by factors of 2000 and 130, respectively. These experiments suggest that the Cys319 loop does indeed have different conformations during the dehydrogenase and hydrolase reactions as suggested by the crystal structures. Importantly, these experiments reveal that the structure of the Cys319 loop modulates the closure of the mobile flap. This conformational change converts the enzyme from a dehydrogenase into hydrolase, suggesting that the conformation of the Cys319 loop may gate the catalytic cycle.

X-ray crystal structures of enzyme−ligand complexes are widely believed to provide snapshots of enzyme−substrate interactions during a catalytic cycle, but such structures may instead depict off-pathway conformations that are not relevant to catalysis. Crystallization conditions introduce a further complication, because pH, ionic strength, and salt composition are seldom physiological, and therefore increase the likelihood that the crystallized conformation is not catalytically relevant. While site-directed mutagenesis is often used to confirm the importance of active site residues, such experiments rarely go beyond the evaluation of k_{cat} and K_m and thus are very blunt probes of residue function and the catalytic competence of a given conformation. Thus, the presumption that X-ray crystal structures of enzyme−ligand complexes mimic catalytic states has seldom been thoroughly scrutinized.

Inosine 5′-monophosphate dehydrogenase (IMPDH)[1] is an excellent system for addressing these questions. This enzyme catalyzes two distinct chemical transformations (Scheme 1; *Tritrichomonas foetus* IMPDH numbering will be used throughout): (1) a dehydrogenase reaction in which the catalytic Cys319 attacks the 2-position of IMP, expelling a hydride to NAD^+ to form the thioimidate E−XMP* intermediate, and (2) a hydrolysis reaction in which the E−XMP* intermediate is converted to XMP. Ten X-ray crystal structures of enzyme−inhibitor complexes of *T. foetus* IMPDH alone have been determined, with resolutions from 2.0 to 2.2 Å, at pH 6.3−8.0, in either polyethylene glycol or sodium malonate as the precipitant (*1*−*5*). These structures suggest that IMPDH undergoes a series of conformational changes during the course of a catalytic cycle (*6*). A large conformational change separates the two chemical reactions: NADH departs after the dehydrogenase reaction, and a mobile flap (residues 412−432) moves into the vacant dinucleotide site, carrying Arg418 into the active site where it acts as a general base to activate water (*7*). This closed conformation is captured in the crystal structure of the E·MZP complex (*2*). Mutations of Arg418 and the neighboring Tyr419 disrupt the hydrolysis step but have no effect on the hydride transfer step, confirming the catalytic relevance of the E·MZP crystal structure (*1*, *8*, *9*).

Two other mobile strutural elements are evident in the crystal structures: the loop that contains the catalytic Cys319 (residues 313−328) and the C-terminal segment (residues 481−503) (Figure 1). The Cys319 loop is trapped in at least three conformations and is also disordered in several other crystals. The C-terminal segment is disordered in most crystals but is found in a loose helix in E·RVP complexes and in an α-helix in E·MZP complexes. With the exception of the E·MZP complex, the catalytic relevance of these structures has not been established.

†This work was supported by National Institutes of Health Grant GM054403 (L.H.).

*To whom correspondence should be addressed: MS009, Brandeis University, 415 South St., Waltham, MA 02454-9110. Phone: (781) 736-2233. Fax: (781) 736-2349. E-mail: hedstrom@brandeis.edu.

[1]Abbreviations: IMP, inosine 5′-monophosphate; XMP, xanthosine 5′-monophosphate; IMPDH, IMP dehydrogenase; TAD, tiazofurin adenine dinucleotide; TAZ, tiazofurin; RVP, ribavirin monophosphate; MPA, mycophenolic acid; MZP, mizoribine monophosphate; PDB, Protein Data Bank.

 Published on Web 11/09/2010

Scheme 1: IMPDH Reaction and Structures of Inhibitors[a]

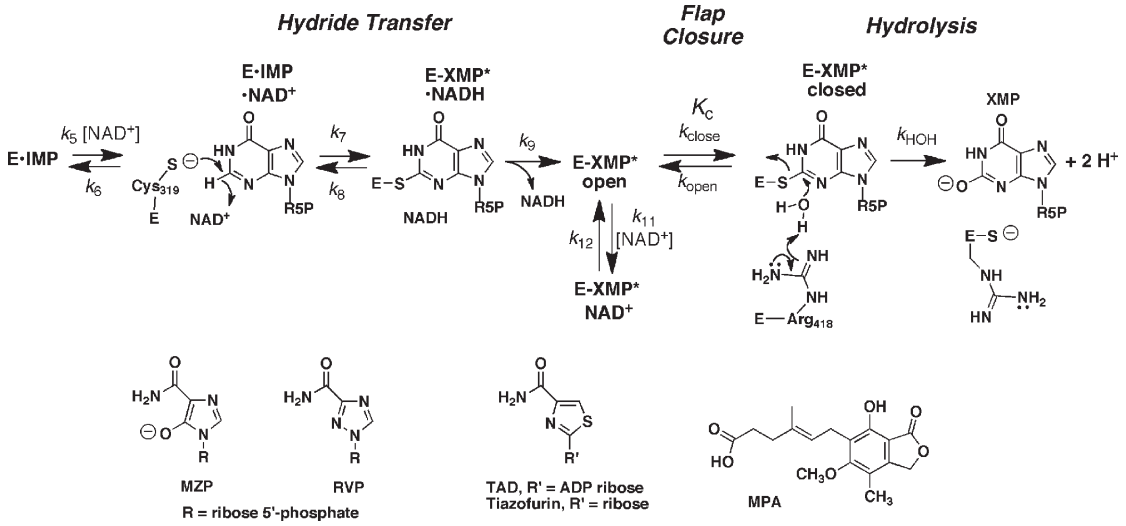

[a]Both the hydride transfer and hydrolysis reactions are likely to be additions and/or eliminations; however, single rate constants can describe these steps because the lifetimes of the tetrahedral intermediates are fleeting. Therefore, the tetrahedral intermediates have been omitted for the sake of clarity. Rate constants as defined previously (*9*, *12*, *14*).

This work addresses the catalytic relevance of the various conformations of the Cys319 loop, so these conformations will be described in more detail.

The entire Cys319 loop is visible in four structures in addition to E·MZP: E·IMP, E·IMP·TAD, E·RVP·MPA, and E·RVP [PDB entries 1ME9, 1LRT, 1ME7, and 1ME8, respectively (Figure 1)] (*1*−*4*). E·RVP·MPA and E·RVP are very similar, so only the E·RVP·MPA conformation will be considered further here. E·IMP·TAD is believed to be a model for E·IMP·NAD^+, while E·RVP·MPA is a possible model for both E−XMP*·NADH* and $E-XMP^*_{open}$. The ends of the Cys319 loop, residues 313−318 and 325−328, are very similar in all of the structures, and the positions of Cys319 and Ile320 change only slightly. In contrast, the position of Arg322 changes dramatically, and Thr321, Glu323, and Gln324 are also found in different positions. The most extreme positions of the side chains of Thr321, Arg322, Glu323, and Gln324 are separated by 8.8, 13, 6.7, and 5.6 Å, respectively. Similar conformations are observed in both E·IMP and E·IMP·TAD, though the side chain of Arg322 is found in different rotamers (Figure 1D,E). Arg322 is solvent-exposed in E·IMP but forms two hydrogen bonds to the carboxamide group of TAD in E·IMP·TAD. A second conformation of the Cys319 loop is found in E·RVP·MPA (Figure1D). The helical arrangement of residues 322−324 has shifted; this segment makes only one hydrogen bond to a protein residue, between Gln324 and Cys319, but this interaction is not likely to be available when Cys319 is part of E−XMP*. The E·RVP·MPA structure is considerably more ordered than E·IMP and E·IMP·TAD; the C-terminal segment is visible, and the monovalent cation binding site is present. The level of order increases in E·MZP. The Cys319 loop makes one turn of an α-helix; the C-terminal segment forms an α-helix, and the flap occupies the dinucleotide site. This Cys319 conformation is stabilized by a hydrogen bonding network that includes five hydrogen bonds with Arg322 (Figure 1E).

These structures suggest the following model for the IMPDH catalytic cycle (Figure 2, path 1). When NAD^+ binds, Arg322 rotates to form two hydrogen bonds that facilitate hydride transfer. Formation of E−XMP* changes the conformation of the Cys319 loop to allow monovalent cation binding and the C-terminal segment to dock; when NADH departs, residues 321−324 and the C-terminal segment form α-helices anchored by Arg322. This new conformation allows the flap to close so that E−XMP* is hydrolyzed. However, the catalytic relevance of these conformations is by no means assured; in addition to the caveats discussed above, Cys319 is oxidized to sulfenic acid in E·IMP, and E·RVP·MPA contains Na^+ instead of K^+. Further, the Cys319 loop has similar conformations in the structures of E·MZP and the E−XMP*·MPA complex of Chinese hamster IMPDH (*2*, *10*), which suggests another plausible alternative (path 2). The Cys319 loop has the same conformation in all E−XMP* complexes, i.e., the conformation found in E·MZP. Path 2 implies that the movement of the flap is independent of the conformation of the Cys319 loop.

If the Cys319 loop has different conformations throughout the catalytic cycle as in path 1, then mutations in residues 321−324 should have disparate effects on the dehydrogenase and hydrolysis steps (Figure 3A). Conversely, if the Cys319 loop has the same conformation in all E−XMP* complexes, these mutations should have similar effects on both steps (Figure 3B). At present, only the Ala mutation of Thr321 has been evaluated in detail (*8*), and this substitution has equivalent effects on both hydride transfer and hydrolysis. However, this mutation removes hydrogen bonding interactions in two conformations of the Cys319 loop, so this result is not informative. Here we have examined the mechanistic consequences of mutations at Arg322, Glu323, and Gln324. The results are consistent with path 1, suggesting that the crystal structures are indeed catalytically relevant. Moreover, these experiments have uncovered communication between the Cys319 loop and the Arg418 flap, suggesting that the conformation of the Cys319 loop may gate the closure of the flap.

MATERIALS AND METHODS

Materials. IMP was purchased from Sigma. NAD^+ was purchased from Roche. DTT was purchased from Research Organics, Inc. Tris, glycerol, EDTA, and KCl were purchased from Fisher Scientific.

Synthesis of [*2-*^{2}*H*]*IMP*. [2-^{2}H]Inosine was synthesized from AICAR and [^{2}H]ethyl-orthoformate and phosphorylated with

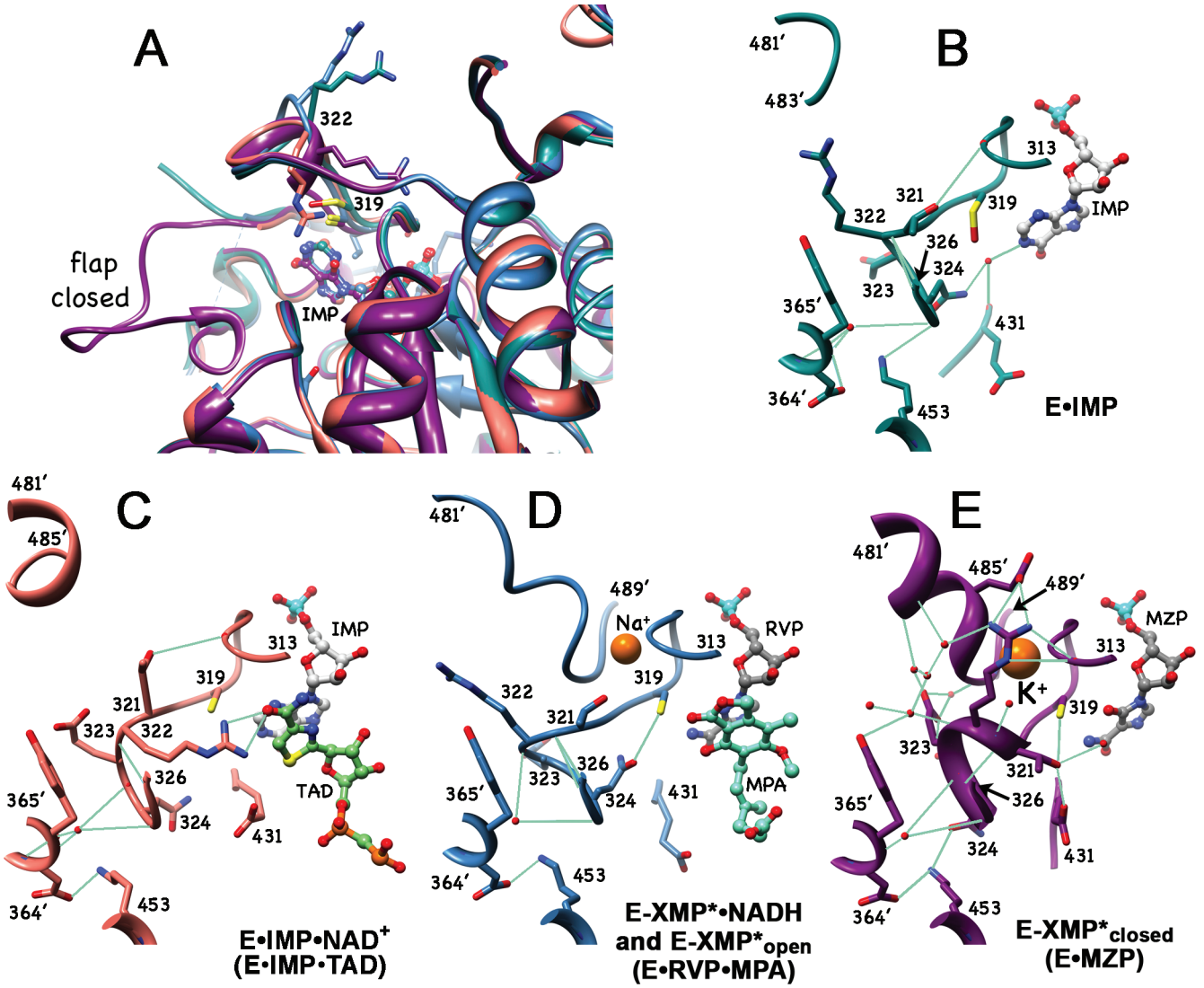

FIGURE 1: Conformations of the Cys319 loop. (A) Overlay of the structures of monomers of E·IMP (cyan, PDB entry 1ME9), E·IMP·TAD (salmon, PDB entry 1LRT), E·RVP·MPA (blue, PDB entry 1ME8), and E·MZP (magenta, PDB entry 1PVN) complexes. Only the side chains of Cys319 and Arg322 are displayed. IMP, RVP, and MZP are displayed; these molecules occupy the same space, so only IMP is labeled. TAD and MPA are omitted for the sake of clarity. The flap is only visible in the E·MZP structure, where it occupies the NAD site. Panels B-E show a different view of the Cys319 loop in these structures. All residues that interact with Arg322, Glu323, and Gln324 are shown; residues from the neighboring monomer are denoted with a prime. All panels display the same set of residues, unless those residues are disordered (e.g., residues 484′−489′ are disordered in the E·IMP complex). Green lines denote hydrogen bonds. IMPDHs are activated by monovalent cations, but the monovalent cation binding site is visible only in the structures of the E·RVP·MPA and E·MZP complexes. (B) E·IMP. (C) E·IMP·TAD, a putative model for E·IMP·NAD^+. (D) E·RVP·MPA, a putative model for the open states of E−XMP*, e.g., E−XMP*·NADH and $E-XMP^*_{open}$. Note that while the segment of residues 481′−489′ has a helical structure, it does not form an α-helix as in the E·MZP complex in the next panel. (E) E·MZP, a model for $E-XMP^*_{closed}$. This figure was produced with UCSF Chimera (*18*).

phosphorus oxychloride in trimethyl phosphate using known procedures as described previously (*11*).

Site-Directed Mutagenesis. The R322A, R322E, Q324A, and E323A mutations were constructed in pTf1, which contains the *Tf*IMPDH gene in the pKK223-3 plasmid (*12*). Point mutations were created using the Quikchange kit (Stratagene, La Jolla, CA). The entire coding sequences were sequenced to ensure that no undesired mutations were introduced (Genewiz, Inc.).

Expression and Purification of IMPDH. The mutant IMPDH genes were expressed in *Escherichia coli* H712 cells, which lack endogenous IMPDH (*13*). All the mutants were purified using IMP affinity column chromatography with buffer A [50 mM Tris (pH 7.5), 1 mM DTT, and 10% glycerol]. IMPDH was eluted with 0.5 mM IMP in buffer A, dialyzed against buffer A to remove IMP, and stored at −20 °C. Purity was >95% as assessed by sodium dodecyl sulfate−polyacrylamide gel electrophoresis (SDS−PAGE). The concentration of IMPDH was determined by Bio-Rad assay using IgG as a standard with a correction factor of 2.6 as previously described (*9*).

Steady-State Kinetics. Standard IMPDH assays were performed in assay buffer [50 mM Tris-HCl (pH 8.0), 100 mM KCl, and 1 mM DTT] at 25 °C. The production of NADH was monitored spectrophotometrically at 340 nm (ε = 6.22 mM^{-1} cm^{-1}). Initial velocities were fit by the Michaelis−Menten equation (eq 1) or an equation including uncompetitive inhibition (eq 2) using SigmaPlot (Systat Software, Inc.) (*12*):

$$v = V_m[S]/(K_m + [S]) \quad (1)$$

$$v = V_m/(1 + K_m/[S] + [S]/K_{ii}) \quad (2)$$

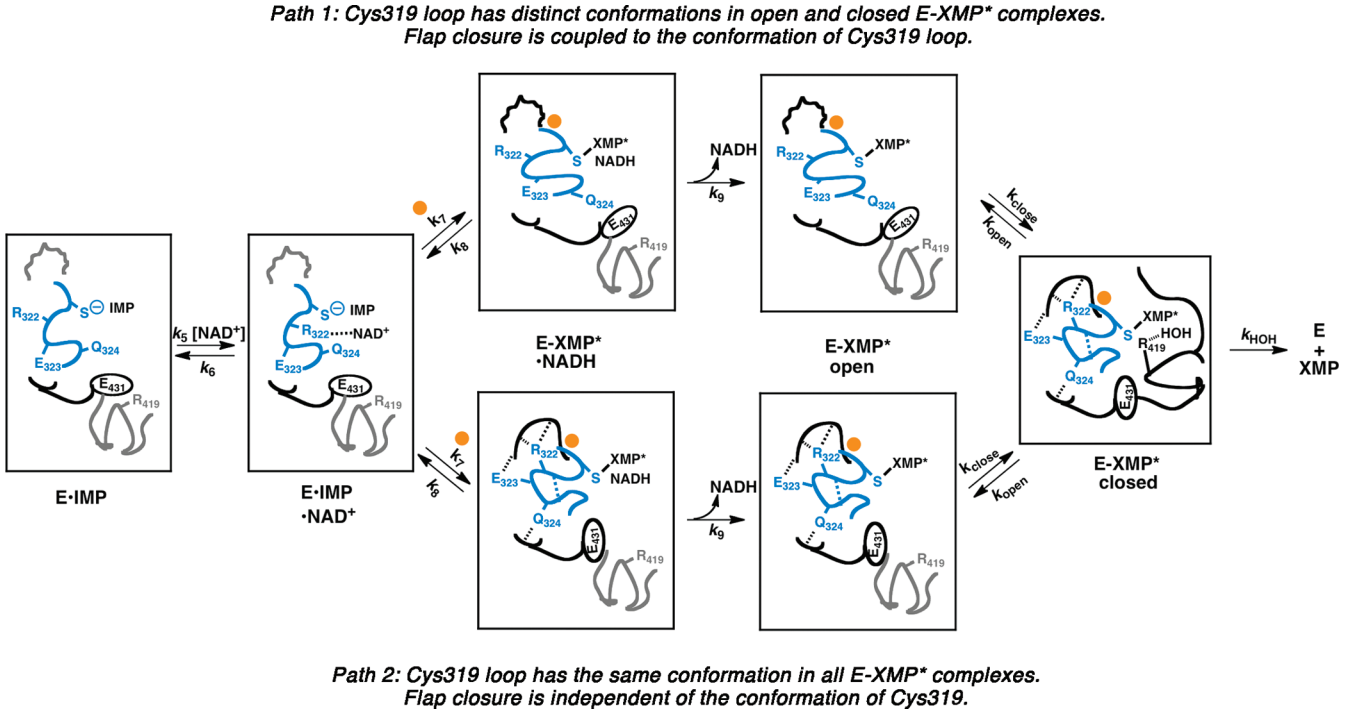

FIGURE 2: Model for conformational transitions of the IMPDH catalytic cycle. The Cys319 loop is colored blue; disordered segments are colored gray, and the monovalent cation is colored orange. The presence of hydrogen bonds is indicated by the dashed lines.

where v is the initial velocity, V_m is the maximal velocity, K_m is the Michaelis constant for the substrate (S), and K_{ii} is the inhibition constant for S.

Pre-Steady-State Kinetics. Pre-steady-state experiments were performed monitoring either NADH absorbance (340 nm) or fluorescence (340 nm excitation, 420 nm cutoff filter). Enzyme (3 μM for R322A, E323A, and Q324A and 1.5 μM for R322E) and saturating IMP (300 μM for R322A, 1.5 mM for R322E, and 1 mM for E323A and Q324A) were preincubated and combined with an equal volume of varying concentrations of NAD^+.

Multiple-Inhibitor Kinetics. Multiple-inhibitor experiments with tiazofurin and ADP were performed as described previously (*9*). Reaction mixtures contained IMP and NAD^+. For R322A, 200 μM IMP and 1 mM NAD^+ were used. For R322E, 500 μM IMP and 1 mM NAD^+ were used. For Q324A, 200 μM IMP and 120 μM NAD^+ were used. For E323A, 1 mM IMP and 350 μM NAD^+ were used. Initial velocities were fitted to eq 3:

$$v = v_0/(1 + [I]/K_i + [J]/K_j + [I][J]/\alpha K_i K_j) \quad (3)$$

where v is the initial velocity, v_0 is the initial velocity in the absence of inhibitor, K_i and K_j are the inhibition constants for inhibitors I and J, respectively, and α is the interaction constant.

Equilibrium Dissociation Constants (K_d). NAD^+ was successively added to 0.2−0.3 μM wild-type or R322E in assay buffer at 25 °C. Protein fluorescence was measured with Hitachi F-2000 fluorescence spectrophotometer. To minimize inner filter effects, an excitation wavelength of 295 nm was used and emission was monitored at 344 nm. Inner filter corrections were calculated by the formula

$$F_c/F_o = \text{antilog}[(A_{ex} + A_{em})/2] \quad (4)$$

where F_c is the corrected fluorescence, F_o is the observed fluorescence, and A_{ex} and A_{em} are the absorbances at the excitation and emission wavelengths, respectively. F_c/F_o was less than 2 for all concentrations. Because purines are fluorescent quenchers, nonspecific quenching was measured via titration of the ligand against a solution of L-tryptophan as previously described (*14*).

RESULTS AND DISCUSSION

Mutant Construction and Initial Characterization. We used site-directed mutagenesis to construct R322A, R322E, E323A, and Q324A. These enzymes were expressed in an *E. coli* strain that lacks the endogenous IMPDH. The enzymes were purified using IMP affinity chromatography, which demonstrates that the mutations did not grossly perturb structure. All of the enzymes were active; steady-state kinetic parameters are listed in Table 1. The mutant enzymes displayed at least 20% activity relative to that of the wild type, with the exception of R322E, which has 0.5% activity. All the mutations increase the value of K_m for IMP (unfortunately, the low activity of R322E precluded the determination of the K_m for IMP), and all except Q324A increase the value of the K_m for NAD^+.

Substitutions of Arg322, Glu323, and Gln324 Perturb the Equilibrium between the Open and Closed Conformations. As described previously (*8*, *9*, *14*, *15*), the equilibrium (K_c) between the open and closed conformations of the flap was probed with multiple-inhibitor experiments. If the closed conformation is favored, the binding of tiazofurin in the nicotinamide subsite will shift the enzyme to the open conformation, increasing the affinity of ADP for the adenosine subsite. This synergistic interaction provides a measure of $E{-}XMP^*_{open}$, and thus of the value of K_c (see the Supporting Information for a detailed explanation). E323A is no longer inhibited by tiazofurin (K_i > 200 mM), so the value of K_c could not be determined for this enzyme.

Synergistic interactions are observed between tiazofurin and ADP for R322A, E323A, and Q324A (Figure 4 and Table 2). Surprisingly, the value of K_c is significantly decreased in all three mutant enzymes (Table 2) even though Arg322, Glu323, and Gln324 do not interact directly with the flap. All three residues participate in extensive hydrogen bonding networks when the

flap is in the closed conformation (Figure 1E) and have few interactions in complexes in which the flap is open (Figure 1B−D). These observations suggest that flap closure requires that the Cys319 loop adopt the conformation of the E·MZP complex. Therefore, the conformation of the Cys319 loop controls the closing of the flap, effectively gating the hydrolysis reaction.

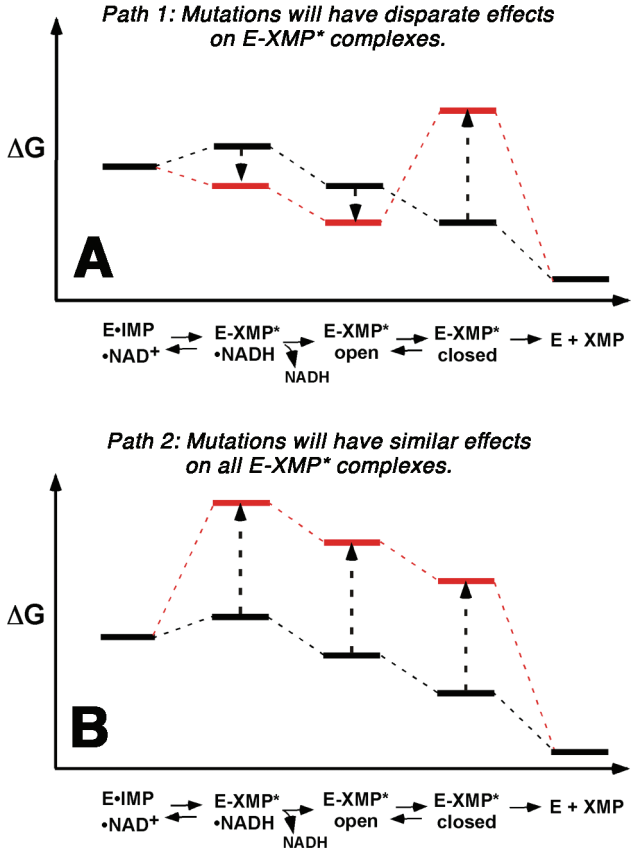

FIGURE 3: Hypothetical effects of mutations on the various complexes in the IMPDH catalytic cycle. The wild-type reaction coordinate is colored black, and the consequences of mutations are colored red. (A) If the Cys319 loop has a different conformation in the open states of E−XMP*, e.g., E−XMP*·NADH and E−XMP*$_{open}$, than in E−XMP*$_{closed}$, then the mutations should have different effects on these states. For example, the R332A mutation removes five hydrogen bonds from E−XMP*$_{closed}$ and so should significantly destabilize this conformation. However, Arg322 is solvent-exposed in the open conformations of E−XMP*, so this mutation should have little effect on these states. (B) If the Cys319 loop has the same conformation in all E−XMP* states, then a mutation that destabilizes E−XMP*$_{closed}$ will destabilize all other states.

Experimental Strategy. A series of isotope effect and pre-steady-state experiments were performed to delineate the effects of these mutations on both chemical transformations. The hydride transfer step was probed by monitoring the reactions with [2-^{2}H]-IMP, while the hydrolysis step was probed by performing the reaction in D_2O. Pre-steady-state reaction progress curves were collected by mixing E·IMP with varying concentrations of NAD^+; experiments monitored NADH production with absorbance and/or fluorescence. The absorbance at 340 nm reports on both E−XMP*·NADH and free NADH. Fortuitously, E−XMP* quenches the fluorescence of NADH in the E−XMP* complex, so only free NADH has a fluorescent signal (excitation wavelength of 340 nm, emission wavelength of 400 nm). The progress curves were initially fit to equations containing single- or

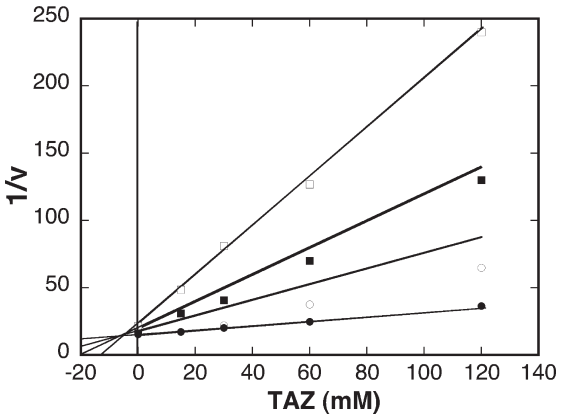

FIGURE 4: Multiple-inhibitor experiment with R322A. ADP concentrations of 0 (●), 2.5 (○), 5 (■), and 10 mM (□).

Table 2: Determination of K_c Values for the *T. foetus* IMPDH Mutants[a]

	K_c	α	K_i(ADP) (mM)	K_i(TAZ) (mM)
wild type[b]	140	0.007 ± 0.002	31 ± 2	69 ± 9
R322A	11	0.08 ± 0.03	17 ± 4	91 ± 18
R322E	na[c]	na[c]	50 ± 40	> 200
E323A	49	0.02 ± 0.02	25 ± 7	300 ± 100
Q324A	6	0.14 ± 0.08	7 ± 2	90 ± 25

[a]The value of the interaction constant α was determined using multiple-inhibitor experiments with tiazofurin (TAZ) and ADP as described in Materials and Methods and Supporting Information. The value of α approximates the fraction of E−XMP*$_{open}$, allowing the calculation of K_c. [b]Data from refs *9* and *17*. [c]Not applicable. No inhibition was observed with tiazofurin in the presence or absence of ADP.

Table 1: Steady-State Kinetic Parameters and Isotope Effects for Reactions of *T. foetus* IMPDH Mutants[a]

	wild type[e]	R322A	R322E	E323A	Q324A
k_{cat} (s^{-1})	1.9 ± 0.2	0.36 ± 0.01	0.009 ± 0.001	1.10 ± 0.03	0.43 ± 0.03
K_m(IMP) (μM)	1.7 ± 0.4	7.6 ± 0.8	nd[g]	31 ± 8	28 ± 6
K_m(NAD^+) (μM)	150 ± 30	910 ± 90	2600 ± 700	300 ± 20	120 ± 20
K_{ii}(NAD^+) (mM)	7 ± 2	na[f]	na[f]	na[f]	2.4 ± 0.3
$^Dk_{cat}$[b]	1.05 ± 0.05	1.5 ± 0.2	2.2 ± 0.8	nd[g]	nd[g]
$^D(k_{cat}/K_m)$[b]	2.0 ± 0.5	2.1 ± 0.1	nd[g]	nd[g]	nd[g]
SIE k_{cat}[c]	1.6 ± 0.1	1.1 ± 0.1	1.5 ± 0.1	2.6 ± 0.2	2.2 ± 0.1
SIE k_{cat}/K_m[c]	0.7 ± 0.1	0.4 ± 0.1	nd[g]	0.6 ± 0.2	1.3 ± 0.7
rate-limiting step(s)[d]	$k_9 + k_{HOH}$	$k_H + k_{close}$	$k_H + k_{HOH}$	k_{HOH}	k_{HOH}

[a]Conditions as described in Materials and Methods. [b]Isotope effect using [2-^{2}H]IMP. [c]Solvent deuterium isotope effect. [d]See Scheme 1: k_9, NADH release; k_H, hydride transfer ($= k_7 + k_8$); k_{close}, flap closure; k_{HOH}, hydrolysis of E−XMP*. [e]Data from ref *12*. [f]Not applicable. No NAD^+ inhibition was observed at concentrations up to 5 mM. [g]No data.

double-exponential and steady-state terms, and the resulting values were used as starting points for global fits to the mechanism of Scheme 1 using Dynafit (*16*). Figure 5 shows the global fit for Q324A as an example; fits for the other enzymes are included in the Supporting Information. The global fits were validated by determining the values of k_{cat}, K_m, and K_{ii} for NAD^+ using the initial rates simulated with the microscopic rate constants; good agreement with the experimental values was obtained in all cases (compare Tables 1 and 3). In addition, the isotope effects were simulated with the assumption that the intrinsic isotope effects are 3, and again the simulated values are in good agreement with experimental values.

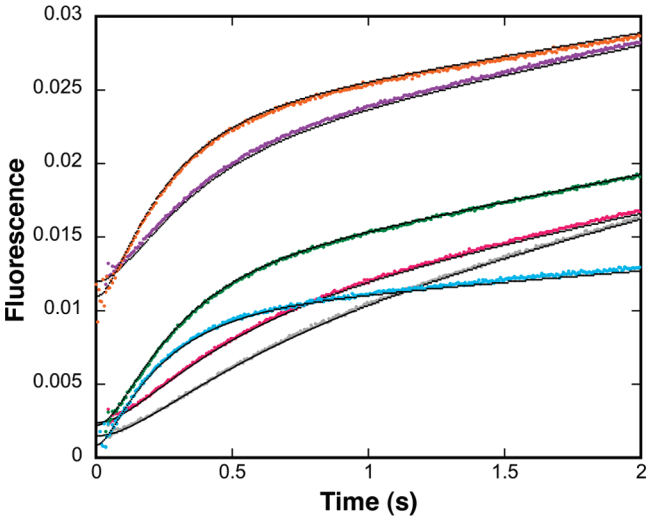

FIGURE 5: Progress curves for the Q324A reaction. The production of NADH was monitored: 3 μM E, 500 μM IMP, and 250 (gray), 500 (pink), 1000 (purple), 2000 (green), 4000 (orange), and 8000 μM NAD^+ (blue). Simulations using the parameters derived in the global data fitting using Dynafit are colored black (Table 3).

Despite the gross similarities in the steady-state parameters of R322A, E323A, and Q324A, each mutation has distinct effects on the microscopic rate constants, as summarized in Figure 6 and described in detail below in order of increasing perturbation. The low activity of R322E permitted only rudimentary characterization of the microscopic rate constants, which nonetheless reveal that this mutation has a large effect on both chemical transformations.

Characterization of E323A. The E323A mutation has only subtle effects on the IMPDH reaction. A burst of NADH is observed in the presteady state, which indicates that the hydride transfer step is fast relative to subsequent steps, as observed with wild-type IMPDH. A somewhat larger SIE is observed than with the wild-type enzyme, which suggests that the hydrolysis step has become more rate-limiting. Global fits of the reaction progress curves substantiate these conclusions (Table 3 and Figure 6): the release of NADH is slightly faster than in wild-type IMPDH, and the hydrolysis step is slightly slower. The global fit uncovers a significant change in the hydride transfer step: the rate ($k_7 + k_8$) decreases by a factor of 4 while the equilibrium (k_7/k_8) increases from 0.6 to 3. Intriguingly, this 5-fold increase in the stability of the E−XMP*·NADH complex is similar in magnitude to the decrease in the value of K_c described above (a factor of 3); both of

Table 3: Microscopic Rate Constants for the Reactions of the IMPDH Mutants[a]

	wild type[b]	R322A,[c] fast conformation	R322A,[d] slow conformation	R322E	E323A	Q324A
NAD^+ on, k_5 ($\times 10^{-3}$ M^{-1} s^{-1})	29 ± 2	5 ± 1	6 ± 1	≥3.5	300 ± 200	32 ± 6
NAD^+ off, k_6 (s^{-1})	4 ± 1	19 ± 3	26 ± 4	≥740 (≥K_m/k_5)	540 ± 390	140 ± 40
forward hydride transfer, k_7 (s^{-1})	34 ± 2	7.5 ± 0.9	7.8 ± 0.8	~0.015	16.3 ± 0.4	41 ± 3
reverse hydride transfer, k_8 (s^{-1})	59 ± 5	5.7 ± 0.8	5.3 ± 0.6	nd[h]	5.2 ± 0.4	3.7 ± 0.4
NADH release, k_9 (s^{-1})	8.5 ± 0.4	2.9 ± 0.3	2.9 ± 0.1	fast	12.7 ± 0.5	4.9 ± 0.2
k_{close}	14000	35 ± 760	1.4 ± 0.3	fast	140 ± 140	30 ± 80
k_{open}	1000	3 ± 25	na[g]	fast	9 ± 5	6 ± 30
NAD^+ inhibition on, k_{11} ($\times 10^{-6}$ M^{-1} s^{-1})	2	0.1 ± 2	0.06 ± 0.5	na[g]	0.06 ± 0.06	0.01 ± 0.02
NAD^+ inhibition off, k_{12} (s^{-1})	27 ± 3	20 ± 500	80 ± 600	na[g]	35 ± 46	7 ± 50
k_{HOH} (s^{-1})	4	1 ± 3	4 (fixed)	0.03	3.4 ± 0.3	0.48 ± 0.01
calculated K_c	na[g]	7	na[g]	na[g]	15	5
simulated $K_m(NAD^+)$ (μM)[d]	110	430	510	na[g]	290	100
simulated k_{cat} (s^{-1})[e]	2.0	0.3	0.3	na[g]	1.8	0.4
simulated $K_{ii}(NAD^+)$ (μM)[d]	4300	> 5000	> 5000	na[g]	> 5000	5000
simulated $^{D}k_{cat}$[e,f]	1.1	1.1	1.1	na[g]	1.3	1
simulated $^{D}k_{cat}/K_m$[e,f]	1.2	1.6	1.9	na[g]	2.6	1
simulated $^{D_2O}k_{cat}$[e,f]	2.1	2.1	1.2	na[g]	2.1	2.5
simulated $^{D_2O}k_{cat}/K_m$[e,f]	1.1	0.6	0.6	na[g]	1.1	0.9

[a]Global fits of the reaction of Scheme 1 were obtained for reaction progress curves for R322A, E323A, and Q324A using Dynafit (*16*). The rate constants of R322E were estimated from the values of k_{cat} and isotope effects, with the assumption that the intrinsic isotope effects equal 3. [b]Values from ref *9*, where the data from *12* were reprocessed using Dynafit. In ref *12*, the values of k_5 and k_6 were assigned from reactions with an inactive mutant. However, the mutation perturbed NAD^+ binding, so we now rely entirely on the global fit to wild-type data. The value of k_{HOH} was measured experimentally in the reaction with acetylpyridine adenine dinucleotide and fixed during the global fit; the values of k_{close} and k_{open} were fixed at aribitrarily fast values such that K_{close} = 140, and the value of k_{11} is increased by a factor of $1 + K_c$ from ref *12* to account for the conformational change. Note that while these values are in good agreement with experiment in the value of k_{cat} and associated isotope effects, they are a rather poor match for isotope effects on k_{cat}/K_m (compare with Table 1). [c]This mechanism assumes that open to closed conformational change is in rapid equilibrium with a K_c of 11. The values of k_{closed}, k_{open}, and k_{12} are unconstrained; equally good fits are obtained as long as these values are fast relative to the other parameters. [d]This mechanism assumes that closing of the flap is partially rate-limiting. The values of k_{open} and k_{HOH} are unconstrained by the data, and equally good fits are obtained as long as $k_{open} \leq 0.1$ and $k_{HOH} \geq 4$. [e]The reactions were simulated using the parameters mentioned above, saturating IMP, and 25, 50, 100, 250, 500, 1000, and 2000 μM NAD^+. The resulting initial velocities were fit to the Michaelis−Menten equation with or without the NAD^+ substrate inhibition term to derive the values of k_{cat}, $K_m(NAD^+)$, and $K_{ii}(NAD^+)$. [f]Assumes intrinsic isotope effects equal to 3, no changes in other steps; note that significant inverse solvent isotope effects are predicted on k_{cat}/K_m because more E−XMP* complex accumulates in the presence of D_2O, which in turn is trapped by NAD^+ in E−XMP*·NAD^+, decreasing the value of K_m. [g]Not applicable. [h]Not determined.

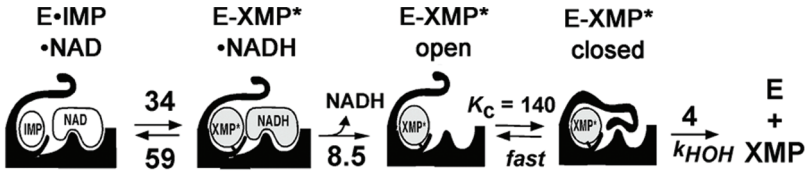

R322A	7.8 5.3	2.9	k_{close} = 1.4	4
R322E	0.015 n.d.	fast	fast	0.03
E323A	16 5	13	49	3.4
Q324A	41 3.7	4.9	6	0.48

FIGURE 6: Effects of the Cys319 loop mutations on the IMPDH reaction. The table is colored according to the magnitude of change induced by the mutation: no color, factor of 1−3; blue, factor of 2−10; green, factor of 10−100; orange, factor of > 100.

these effects can be explained if this mutation stabilizes open conformations of E−XMP* relative to E−XMP*$_{closed}$ as illustrated in Figure 3A. This result is consistent with the X-ray crystal structures: Glu323 makes hydrogen bonds to water molecules in the closed conformation of the E·MZP complex but is solvent-exposed in the other X-ray crystal structures (Figure 1). Therefore, these results are consistent with path 1.

Characterization of Q324A. The Q324A mutation also has fairly subtle effects on the IMPDH reaction. As with E323A, a burst of NADH production is present in the presteady state; a larger SIE is observed, suggesting that the hydrolysis step has become even more rate-limiting. Global fits of the reaction progress curve reveal that while this mutation decreases the rate of the hydride transfer step by a factor of 2, and the value of k_{HOH} decreases by a factor of 8. Like E323A, this mutation increases the equilibrium for hydride transfer to 10. Again, the magnitude of this change is similar to the change in K_c (a factor of 12), suggesting that this substitution also stabilizes the open conformations of E−XMP* as in Figure 3A. As described above, these results are generally consistent with the structural information. Gln324 is solvent-exposed in the E·IMP·TAD complex (Figure 1C), which suggests that residue is not involved in the hydride transfer reaction. In contrast, Gln324 makes two hydrogen bonds in the structure of the E·MZP complex, one of which is to a structural water that makes two additional hydrogen bonds to protein residues (Figure 1E). Therefore, these findings are also consistent with path 1.

Characterization of R322A. When [2-^{2}H]IMP was the substrate, a small isotope effect was observed on k_{cat}, suggesting that hydride transfer may be partially rate-limiting. A burst of free NADH is observed in the presteady state when the reaction is monitored with fluorescence, indicating that a step subsequent to NADH release must be rate-limiting. Surprisingly, no solvent deuterium isotope effect was observed for the reaction of R322A, indicating that the hydrolysis step is no longer rate-limiting. The only likely rate-limiting step remaining is k_{close}, the closure of the flap.

Global fits of the reaction progress curves to two mechanisms were performed; the first assumed that the conformational change is fast, and the second assumed that k_{close} is rate-limiting. Good fits to both mechanisms were obtained (Table 3), and the values of k_{cat}, K_m(NAD$^+$), and K_{ii}(NAD$^+$) derived from both mechanisms were in good agreement with experimental values. However, a significant SIE is expected on k_{cat} when the conformational change is fast, but a SIE is not observed experimentally. When the conformational change is slow, a small SIE on k_{cat} is predicted. Therefore, these results suggest that the substitution of Arg322 with Ala has a profound effect on the rate of flap closure (Figure 6). The global fit also indicates that the R322A mutation significantly perturbed the rate of hydride transfer, though perhaps not as much as would be expected if two hydrogen bonds are lost to the carboxamide group of NAD$^+$. Thus, these results provide further support for path 1 but cast some doubt on the catalytic relevance of the E·IMP·TAD complex.

Characterization of R322E. We constructed and characterized R322E to gain further insight into the role of Arg322. This substitution will clearly disrupt the hydrogen bonding network that stabilizes the E−XMP*$_{closed}$ structure and should thus slow the hydrolysis step. If the interaction between Arg322 and NAD$^+$ is part of the catalytic cycle, this substitution will also profoundly perturb hydride transfer. In contrast, if Arg322 is solvent-exposed during hydride transfer as in the E·IMP structure, then this substitution may have have a modest effect on hydride transfer.

Unlike the other IMPDH mutants, R322E dramatically decreased the value of k_{cat}, by a factor of 200. A SIE is observed on k_{cat}, suggesting that the hydrolysis step is partially rate-limiting. A significant $^D k_{cat}$ is also observed, indicating that hydride transfer is also partially rate-limiting. Assuming intrinsic isotope effects of ~3 on both steps, the values for k_7 is ~0.015 and that for k_{HOH} is ~0.03, indicating that this mutation decreases the rate of hydride transfer by a factor of 2000 and the rate of hydrolysis by a factor of 130. These results are consistent with path 1 and suggest that Arg322 may play an important role in hydride transfer as implied by the E·IMP·TAD complex.

The binding of NAD$^+$ was monitored via intrinsic protein fluorescence to further probe the defect in hydride transfer. We previously reported that the NAD$^+$ binding curve for the wild-type enzyme was sigmoidal and best fit a model with two binding constants (*12*). However, the binding curve becomes hyperbolic with a correction for nonspecific quenching (*14*), with a K_d of 27 ± 6 μM. NAD$^+$ binds to R322E with similar affinity (K_d = 37 ± 10 μM). ADP also binds to both wild-type and mutant enzymes with similar affinity (Table 2). In contrast, the mutation decreases the affinity of tiazofurin by a factor of > 3. These observations suggest that while NAD$^+$ still binds to R322A, the nicotinamide is no longer positioned correctly for efficient hydride transfer, providing further evidence of the catalytic relevance of the E·IMP·TAD structure.

Implications for the Catalytic Cycle of IMPDH. X-ray crystal structures of enzyme−ligand complexes are generally

presumed to provide snapshots of the catalytic cycle. In the case of IMPDH, two plausible models arise from the structures (Figure 3). In path 1, the conformation of the Cys319 loop gates flap closure, while the flap movement is independent of the Cys319 loop conformation in path 2. The experiments described above find that mutations of Arg322, Glu323, and Gln324 have differential effects on hydride transfer, flap closure, and hydrolysis that are most consistent with path 1. These results provide evidence of the catalytic relevance of the E·IMP·TAD, E·RVP, and E·RVP·MPA structures.

ACKNOWLEDGMENT

We thank Thomas Riera for many helpful discussions.

SUPPORTING INFORMATION AVAILABLE

A description of the determination of K_c and figures showing the global fits for the progress curves of the R322A and E323A reactions. This material is available free of charge via the Internet at http://pubs.acs.org.

REFERENCES

1. Gan, L., Petsko, G. A., and Hedstrom, L. (2002) Crystal structure of a ternary complex of *Tritrichomonas foetus* inosine 5′-monophosphate dehydrogenase: NAD^+ orients the active site loop for catalysis. *Biochemistry 41*, 13309–13317.
2. Gan, L., Seyedsayamdost, M. R., Shuto, S., Matsuda, A., Petsko, G. A., and Hedstrom, L. (2003) The immunosuppressive agent mizoribine monophosphate forms a transition state analog complex with IMP dehydrogenase. *Biochemistry 42*, 857–863.
3. Prosise, G. L., and Luecke, H. (2003) Crystal Structures of *Tritrichomonas foetus* Inosine Monophosphate Dehydrogenase in Complex with Substrate, Cofactor and Analogs: A Structural Basis for the Random-in Ordered-out Kinetic Mechanism. *J. Mol. Biol. 326*, 517–527.
4. Prosise, G. L., Wu, J. Z., and Luecke, H. (2002) Crystal Structure of *Tritrichomonas foetus* Inosine Monophosphate Dehydrogenase in Complex with the Inhibitor Ribavirin Monophosphate Reveals a Catalysis-dependent Ion-binding Site. *J. Biol. Chem. 277*, 50654–50659.
5. Whitby, F. G., Luecke, H., Kuhn, P., Somoza, J. R., Huete-Perez, J. A., Philips, J. D., Hill, C. P., Fletterick, R. J., and Wang, C. C. (1997) Crystal structure of *Tritrichomonas foetus* inosine-5′-monophosphate dehydrogenase and the enzyme-product complex. *Biochemistry 36*, 10666–10674.
6. Hedstrom, L., and Gan, L. (2006) IMP dehydrogenase: Structural schizophrenia and an unusual base. *Curr. Opin. Chem. Biol. 10*, 520–525.
7. Hedstrom, L. (2009) IMP Dehydrogenase: Structure, mechanism and inhibition. *Chem. Rev. 109*, 2903–2928.
8. Guillén Schlippe, Y. V., and Hedstrom, L. (2005) Is Arg418 the Catalytic Base Required for the Hydrolysis Step of the IMP Dehydrogenase Reaction? *Biochemistry 44*, 11700–11707.
9. Guillén Schlippe, Y. V., Riera, T. V., Seyedsayamdost, M. R., and Hedstrom, L. (2004) Substitution of the Conserved Arg-Tyr Dyad Selectively Disrupts the Hydrolysis Phase of the IMP Dehydrogenase Reaction. *Biochemistry 43*, 4511–4521.
10. Sintchak, M. D., Fleming, M. A., Futer, O., Raybuck, S. A., Chambers, S. P., Caron, P. R., Murcko, M., and Wilson, K. P. (1996) Structure and mechanism of inosine monophosphate dehydrogenase in complex with the immunosuppressant mycophenolic acid. *Cell 85*, 921–930.
11. Wang, W., and Hedstrom, L. (1997) The kinetic mechanism of human inosine 5′-monophosphate type II: Random addition of substrates, ordered release of products. *Biochemistry 36*, 8479–8483.
12. Digits, J. A., and Hedstrom, L. (1999) Kinetic mechanism of *Tritrichomonas foetus* inosine-5′-monophosphate dehydrogenase. *Biochemistry 38*, 2295–2306.
13. Nijkamp, H. J. J., and De Haan, P. G. (1967) Genetic and biochemical studies of the guanosine 5′-monophosphate pathway in *Escherichia coli*. *Biochim. Biophys. Acta 145*, 31–40.
14. Riera, T. V., Wang, W., Josephine, H. R., and Hedstrom, L. (2008) A kinetic alignment of orthologous inosine-5′-monophosphate dehydrogenases. *Biochemistry 47*, 8689–8696.
15. Kohler, G. A., Gong, X., Bentink, S., Theiss, S., Pagani, G. M., Agabian, N., and Hedstrom, L. (2005) The functional basis of mycophenolic acid resistance in *Candida albicans* inosine-5′-monophosphate dehydrogenase. *J. Biol. Chem. 280*, 11295–11302.
16. Kuzmic, P. (1996) Program DYNAFIT for the analysis of enzyme kinetic data: Application to HIV proteinase. *Anal. Biochem. 237*, 260–273.
17. Digits, J. A., and Hedstrom, L. (2000) Drug selectivity is determined by coupling across the NAD^+ site of IMP dehydrogenase. *Biochemistry 39*, 1771–1777.
18. Pettersen, E. F., Goddard, T. D., Huang, C. C., Couch, G. S., Greenblatt, D. M., Meng, E. C., and Ferrin, T. E. (2004) UCSF Chimera: A visualization system for exploratory research and analysis. *J. Comput. Chem. 25*, 1605–1612.